Biallelic Mutations in *ADPRHL2*, Encoding ADP-Ribosylhydrolase 3, Lead to a Degenerative Pediatric Stress-Induced Epileptic Ataxia Syndrome

Shereen G. Ghosh,[1,2] Kerstin Becker,[3,4,5] He Huang,[6,7] Tracy D. Salazar,[1,2] Guoliang Chai,[1,2] Vincenzo Salpietro,[8] Lihadh Al-Gazali,[9] Quinten Waisfisz,[10] Haicui Wang,[3,4,5] Keith K. Vaux,[11] Valentina Stanley,[1,2] Andreea Manole,[8] Ugur Akpulat,[3,4,12] Marjan M. Weiss,[10] Stephanie Efthymiou,[8] Michael G. Hanna,[8] Carlo Minetti,[13] Pasquale Striano,[13] Livia Pisciotta,[14] Elisa De Grandis,[14] Janine Altmüller,[15] Peter Nürnberg,[15] Holger Thiele,[15] Uluc Yis,[16] Tuncay Derya Okur,[16] Ayse Ipek Polat,[16] Nafise Amiri,[17] Mohammad Doosti,[18] Ehsan Ghayoor Karimani,[18,19] Mehran B. Toosi,[20] Gabriel Haddad,[6,7] Mert Karakaya,[21] Brunhilde Wirth,[5,21] Johanna M. van Hagen,[10] Nicole I. Wolf,[22] Reza Maroofian,[19] Henry Houlden,[8] Sebahattin Cirak,[3,4,5,*] and Joseph G. Gleeson[1,2,*]

ADP-ribosylation, the addition of poly-ADP ribose (PAR) onto proteins, is a response signal to cellular challenges, such as excitotoxicity or oxidative stress. This process is catalyzed by a group of enzymes referred to as poly(ADP-ribose) polymerases (PARPs). Because the accumulation of proteins with this modification results in cell death, its negative regulation restores cellular homeostasis: a process mediated by poly-ADP ribose glycohydrolases (PARGs) and ADP-ribosylhydrolase proteins (ARHs). Using linkage analysis and exome or genome sequencing, we identified recessive inactivating mutations in *ADPRHL2* in six families. Affected individuals exhibited a pediatric-onset neurodegenerative disorder with progressive brain atrophy, developmental regression, and seizures in association with periods of stress, such as infections. Loss of the *Drosophila* paralog *Parg* showed lethality in response to oxidative challenge that was rescued by human *ADPRHL2*, suggesting functional conservation. Pharmacological inhibition of PARP also rescued the phenotype, suggesting the possibility of postnatal treatment for this genetic condition.

ADP-ribosylation is a tightly regulated posttranslational modification of proteins involved in various essential physiological and pathological processes, including DNA repair, transcription, telomere function, and apoptosis.[1–3] The addition of poly-ADP-ribose (PAR) is mediated by a group of enzymes, referred to as poly(ADP-ribose) polymerases (PARPs), in response to cellular stressors, such as excitotoxicity or reactive oxygen species. PARylated proteins can subsequently initiate cellular stress response pathways. After resolution of the original insult, ADP-ribose polymers are rapidly removed.[4,5] Although PAR modification can protect the cell from death in the setting of cellular stress, excessive PAR accumulation or failure to reverse PAR modification can trigger a cell-death response cascade.[6,7]

Humans have two genes encoding specific PAR-degrading enzymes: *ADPRHL2* (MIM: 610624; Gene ID: 54936) and *PARG* (MIM: 603501). Both are capable of hydrolyzing the glycosidic bond between ADP-ribose moieties and are ubiquitously expressed.[8,9] *ADPRH* (MIM: 603081) and putatively *ADPRHL1* (MIM: 610620) encode proteins that can cleave mono-ADP-ribosylated residues and thus are not functionally redundant with *ADPRHL2* and *PARG*.[8] Studies of *in situ* hybridization have shown high *Adprhl2* expression in the developing mouse forebrain and that its expression remains high in the cerebellum, cortex, hippocampus, and olfactory bulb in early postnatal ages and persists into adulthood.[10] $Parg^{-/-}$ mice die embryonically as a result of PAR accumulation and cellular apoptosis.[11] There are no reports of $Adprhl2^{-/-}$ animals,

[1]Laboratory for Pediatric Brain Disease, Howard Hughes Medical Institute, University of California, San Diego, La Jolla, CA 92093, USA; [2]Rady Children's Institute for Genomic Medicine, Rady Children's Hospital, San Diego, CA 92123, USA; [3]Center for Molecular Medicine Cologne, Cologne, Germany; [4]Department of Pediatrics, University Hospital of Cologne, Cologne, Germany; [5]Center for Rare Diseases, Cologne 50937, Germany; [6]Department of Pediatrics, University of California, San Diego, La Jolla, CA 92093, USA; [7]Rady Children's Hospital, San Diego, CA, USA; [8]Department of Neuromuscular Diseases and Neurogenetics Laboratory, University College of London, London WC1E 6BT, UK; [9]Department of Pediatrics, United Arab Emirates University and Tawam Hospital, PO Box 15551, Al Ain, Abu Dhabi, UAE; [10]Amsterdam UMC, Vrije Universiteit Amsterdam, Department of Clinical Genetics, De Boelelaan 1117, Amsterdam, the Netherlands; [11]Division of Medical Genetics, Department of Medicine, School of Medicine, University of California, San Diego, San Diego, CA 92093, USA; [12]Kastamonu University, Medical Faculty, 37150 Kastamonu, Turkey; [13]Pediatric Neurology and Muscular Diseases Unit, Istituto Giannina Gaslini, Department of Neurosciences, Rehabilitation, Ophthalmology, Genetics, and Maternal and Children's Sciences, University of Genoa, Genoa 16126, Italy; [14]Child Neuropsychiatry Unit, Istituto Giannina Gaslini, Department of Neurosciences, Rehabilitation, Ophthalmology, Genetics, and Maternal and Children's Sciences, University of Genoa, Genoa 16126, Italy; [15]Cologne Center for Genomics, University of Cologne, Cologne 50931, Germany; [16]Department of Pediatrics, Division of Child Neurology, Dokuz Eylül University School of Medicine, İzmir 35340, Turkey; [17]Targeted Drug Delivery Research Center, Pharmaceutical Technology Institute, University of Medical Sciences, Mashhad 15731, Iran; [18]Next Generation Genetic Clinic, Mashhad 15731, Iran; [19]Molecular and Clinical Sciences Institute, St. George's, University of London, Cranmer Terrace, London SW17 0RE, UK; [20]Pediatric Neurology, Department of Pediatric Diseases, Faculty of Medicine, Mashhad University of Medical Sciences, Mashhad 15731, Iran; [21]Institute of Human Genetics, Center for Molecular Medicine, and Center for Rare Diseases, University of Cologne, Cologne 50937, Germany; [22]Department of Child Neurology, VU University Medical Center and Amsterdam Neuroscience, Amsterdam 1117, the Netherlands
*Correspondence: sebahattin.cirak@uk-koeln.de (S.C.), jogleeson@ucsd.edu (J.G.G.)
https://doi.org/10.1016/j.ajhg.2018.07.010.

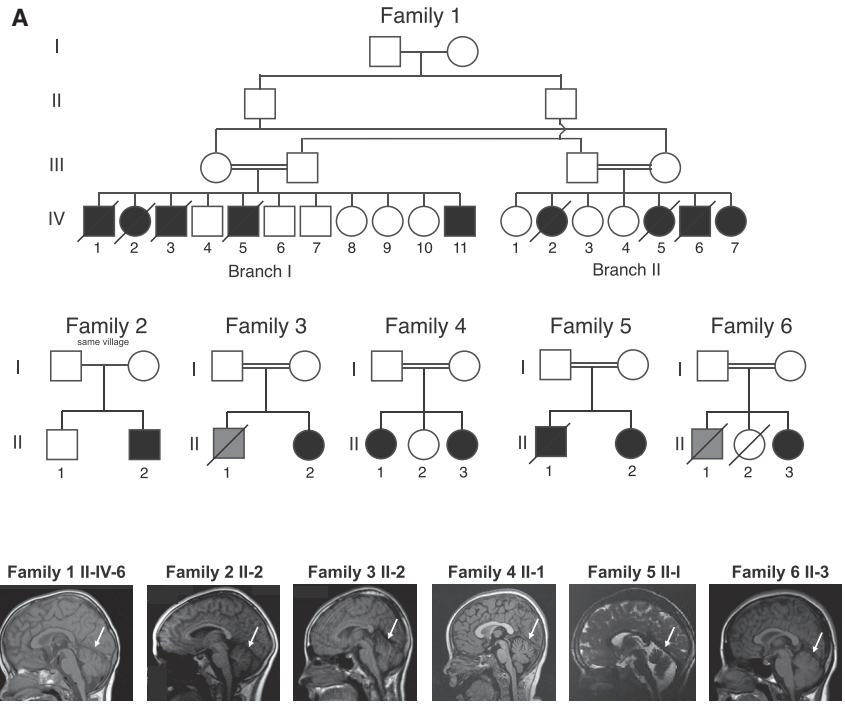

Figure 1. Pedigrees of Families with Mutations in *ADPRHL2* and Their Clinical Presentation

(A) Pedigrees of families 1–6 show consanguineous unions (double bar) and a total of 16 affected individuals. Slashes represent deceased individuals. Black shading indicates affected individuals. Gray shading indicates individuals who passed away from SUDEP; however, no DNA is available.

(B) Panels show midline sagittal MRI for one affected individual from each of the six families. White arrows indicate cerebellar atrophy, evidenced by widely spaced cerebellar folia.

but *Adprhl2*$^{-/-}$ mouse embryonic fibroblasts (MEFs) engineered to express the catalytic domain of nuclear PARP1 in mitochondria show PAR accumulation, as well as longer mitochondrial PAR polymers.[12,13]

Drosophila melanogaster has a single *Parg*-like gene, and null flies are lethal in the larval stage; however, when grown at a permissive temperature, a few can survive. The surviving flies display PAR accumulation, neurodegeneration, reduced locomotion, and premature death,[14] suggesting increased neuronal vulnerability to PAR accumulation. Although mutations in enzymes PARG and PARP have not been reported in human disease, other members of this pathway have been implicated in human phenotypes.[15] For example, mutations in *XRCC1* (MIM: 194360), encoding a molecular scaffold protein involved in complex assembly during the repair of DNA-strand breaks, lead to PARP-1 overactivation and are associated with cerebellar ataxia, ocular motor apraxia, and axonal neuropathy.[16]

In this study, we show that mutations in *ADPRHL2* underlie an age-dependent recessive epilepsy-ataxia syndrome initiating with sudden severe seizures in otherwise healthy individuals followed by progressive loss of milestones, brain atrophy, and death in childhood. We describe six independent families carrying *ADPRHL2* mutations leading to a nearly identical epilepsy-ataxia syndrome (Figure 1A). One of the six families (family 2) lacked documentation of parental consanguinity, and the parents from this family were from the same small village. The clinical details of subjects from all included families are shown in Table 1, and detailed clinical history is narrated in the Supplemental Note. The emerging clinical picture is one of a stress-induced neurodegenerative disease of variable progression with developmental delay, intellectual disability, mild cerebellar atrophy (Figure 1B), and recurring seizures.

Genome-wide linkage analysis of 14 members of family 1 mapped the disease locus to an 11 Mb locus in chromosomal region 1p36 with a genome-wide-significant multipoint LOD score of 3.4 (Figure S1A). Exome sequencing of individual II-IV-6 at >30× read depth for 96.9% of the exome revealed a single rare (allele frequency < 1:1,000) potentially deleterious variant within the linkage interval: a frameshift *ADPRHL2* mutation that segregated with the phenotype according to a recessive mode of inheritance.

Using GeneMatcher, this international collaborative group of authors identified further pathogenic alleles in *ADPRHL2*.[17] After obtaining informed consent from all participating individuals in accordance with the ethical standards of the responsible committee on human experimentation at the University of California, San Diego, we identified a total of six distinct mutations in ADP-ribosylhydrolase-like 2 (*ADPRHL2* [Gene ID: 54936]) in the six families by whole-exome or genome sequencing (see Supplemental Data). All variants were prioritized by allele frequency, conservation, blocks of homozygosity, and predicted effect on protein function (see Supplemental Data), and in all families the homozygous variant in *ADPRHL2* was the top candidate. Variants were confirmed by Sanger sequencing and segregated with the phenotype according to a recessive mode of inheritance. All variants were predicted to be disease causing by MutationTaster.[18] These variants were not encountered in dbGaP, the ExAC Browser, 1000 Genomes, genomAD, or the Greater Middle East Variome.

ADPRHL2 contains six coding exons, yielding a single protein-coding transcript, ADP-ribosylhydrolase 3 (ARH3) (Figure 2A). The encoded 363 amino acid ARH3 is predicted to have a mitochondrial localization sequence and single enzymatic ADP-ribosyl-glycohydrolase domain (Figure 2B). Family 1 carried the homozygous exon 6 mutation c.1000C>T (GenBank: NM_017825), which

introduces a premature stop codon (p.Gln334Ter) predicted to truncate the highly conserved last 30 amino acids of the protein, including part of the ADP-ribosylhydrolase domain. Family 2 harbored the homozygous exon 3 mutation c.316C>T (GenBank: NM_017825), which also introduces a premature stop codon (p.Gln106Ter) in the ADP-ribosylhydrolase domain. Family 3 revealed the homozygous exon 2 missense mutation c.235A>C (GenBank: NM_017825), which leads to an amino acid change (p.Thr97Pro) in a residue that is highly conserved among vertebrates (Figure S2A). Using a previously published crystal structure of ARH3, we localized this residue to an α-helical loop within the ADP-ribosylhydrolase domain and the substrate binding site, which is defined by the position of two Mg^{2+} ions located in adjacent binding sites; thus, the residue is predicted to affect protein structure and enzymatic activity (Figure S2B).[19] Family 4 carried the homozygous 5 bp, exon 3 deletion c.414_418TGCCC (GenBank: NM_017825), which results in a frameshift (p.Ala139GlyfsTer5) in the ADP-ribosylhydrolase domain. Family 5 carried the homozygous exon 4 missense mutation c.530C>T (GenBank: NM_017825), which leads to an amino acid change (p.Ser177Leu) that is also highly conserved among vertebrates. It is localized in a critical α-helical loop within the ADP-ribosylhydrolase domain, also suggesting an effect on protein structure and activity. Family 6 carried the homozygous exon 1 missense mutation c.100G>A (GenBank: NM_017825), which leads to an amino acid change (p.Asp34Asn) that is highly conserved among vertebrates. This change is also localized in a critical α-helical loop within the ADP-ribosylhydrolase domain, suggesting a potential impact on protein structure and activity.

The emerging phenotype of recessive *ADPRHL2* mutations is a degenerative pediatric-onset stress-induced epileptic-ataxia syndrome. Individuals with mutations in this gene are asymptomatic early after birth but gradually develop a cyclic pattern of illness-related spontaneous epileptic seizures or present with a neurodegenerative course including weakness, ataxia, and loss of milestones followed by clinical deterioration that ultimately leads to premature death. Most of the subjects succumbed to sudden unexpected death in epilepsy (SUDEP) or an apnoic-attack-like clinical presentation, suggesting a hyperacute presentation prior to the family's recognition of a predisposition. We could not establish an obvious genotype-phenotype correlation given that we show below that the missense mutation also leads to a severe loss of function. Thus, the clinical variability in the age of onset might occur because the genetic background or environmental challenges lead to variable susceptibility to illness-related cellular stress.

The differential diagnosis for this condition was based upon the presentation of a recessive condition with recurrent exacerbations and predominant features of global developmental delay, intellectual disability, seizures, neurogenic changes on electromyography, hearing impairment, regression, and mild cerebellar atrophy but not microcephaly or cataracts. The differential diagnosis in our families included mitochondrial disorders, spastic ataxia, and peripheral neuropathy.

To determine the impact of these mutations on protein folding and binding activity, we generated recombinant proteins in *E.coli* and purified them by His-tag affinity chromatography. Our results showed that the p.Gln334Ter protein was not evident in the soluble fraction, whereas the wild-type (WT) was recovered with good purity (Figure S3A). The p.Thr79Pro protein was expressed and soluble, although possibly recovered with slightly less purity than WT ARH3. We studied the deleterious impact of p.Thr79Pro by using circular dichroism spectroscopy (Figures S3B and S3C). Compared with the WT, this mutant exhibited reduced α-helical content and an altered secondary structure, in agreement with the fact that p.Thr79Pro occurred within an α-helical domain. Further, the melting temperature (T_m) of p.Thr79Pro was reduced by more than 10°C, confirming destabilization of the mutant (Figures S3D–S3F). We also found that in contrast to WT ARH3, the p.Thr79Pro protein was not stabilized by ligands such as adenosine diphosphate ribose (ADPr) (Figures S3G–S3I). We confirmed the specificity of this assay by using adenosine triphosphate (ATP) and ribose-5-phosphate as negative controls, which were not predicted to bind or stabilize ARH3. Together, these data suggest that both disease-causing, truncating mutants and amino acid substitutions should be destabilized when expressed in cells.

Because the c.1000C>T (p.Gln334ter) mutation of family 1 was in the last exon, we first excluded nonsense-mediated decay (NMD) of the mutant mRNA. We collected skin biopsies from the father (III-II) and two affected individuals (II-IV-6 and II-IV-7), generated primary fibroblasts, and then performed RT-PCR by using primers designed to amplify the last three exons of *ADPRHL2* (Figure S1B). The father's and affected individuals' cells revealed a band of the expected size and of similar intensity to that of a healthy control individual, arguing against NMD. However, when we used an antibody recognizing amino acids 231–245, lysates derived from the affected individuals showed no detectable ARH3 (Figure 2C; Supplemental Data), consistent with a null effect of the truncating mutation. Further, western blot analysis of individual II-2 from family 2 showed an absence of the protein, as predicted by the early stop codon. Fibroblasts from individual II-1 from family 3 showed a severely reduced amount of ARH3 (Figure 2C), consistent with the thermal instability of this mutant protein (Figures S3D–S3F) and the severe alteration of its secondary structure (Figures S3B and S3C).

Whereas humans have two known genes with specific PARG activity (*PARG* and *ADPRHL2*; Figure 3A), *Drosophila* have a single gene that regulates this process: *Parg*. Using the Gal4-UAS system to drive RNAi expression, we found that *Parg* knockdown led to a 60% decrease in total *Parg* mRNA for flies with the ubiquitous *da* promoter and a

Table 1. Mutations in *ADPRHL2* Cause Various Phenotypes, Including Developmental Delay, Cerebellar Atrophy, Ataxia, and Epilepsy

	Family 1							
	I-IV-1	**I-IV-2**	**I-IV-3**	**I-IV-5**	**I-IV-11**	**II-IV-2**	**II-IV-5**	**II-IV-6 (A1)**
Gender	M	F	M	M	M	F	F	M
Country of origin	UAE	UAE	UAE	UAE	UAE	UAE	UAE	UAE
Parental consanguinity	+	+	+	+	+	+	+	+
Current age or age of death	died at 4 years	died at 2 years	died at 7 years	died at 15 years	4 years	died at 2 years	died at 2 years	died at 9 years
Circumstances of death	in sleep	in sleep	seizure	respiratory failure	–	in sleep 1 week after flu-like illness	seizure after playing	respiratory failure after long airplane trip
Mutation								
Genomic (hg19[a])	g.36558895C>T	g.36558895C>T	g.36558895C>T	g.36558895C>T	g.36558895C>T	g.36558895C>T	g.36558895C>T	g.36558895C>T
cDNA	c.1000C>T	c.1000C>T	c.1000C>T	c.1000C>T	c.1000C>T	c.1000C>T	c.1000C>T	c.1000C>T
Protein	p.Gln334*	p.Gln334*	p.Gln334*	p.Gln334*	p.Gln334*	p.Gln334*	p.Gln334*	p.Gln334*
Homozygosity	+	+	+	+	+	+	+	+
Perinatal History								
Normal birth	+	+	+	+	+	+	+	+
Normal early development	+	+	+	+	+	+	+	+
Psychomotor Development								
Speech development	spoke in sentences but then deteriorated	few words at 2 years	normal until 2.5 years but then no further development	normal until 3.5 years but then deteriorated	speaks only a few words	normal speech until death	normal speech until death	normal until 25 years but then deteriorated
Motor development	normal but then deteriorated	normal until death	normal but then deteriorated	normal but then deteriorated	normal but then deteriorated	normal but then deteriorated	normal until death	normal but then deteriorated by 2 years
Seizures								
Seizure onset	18 months	19 months	19 months	24 months	15 months	24 months	15 months	18 months
Seizure types	GTCS	GTCS	GTCS	GTCS	absence, GTCS	GTCS	GTCS	absence, GTCS
Neurological Examination								
Intellect	normal but then delayed	normal until death	normal but then delayed	normal but then delayed	normal but then delayed	normal until death	normal until death	normal but then delayed
EEG	–	–	–	–	–	–	–	generalized epileptiform activity, slow background
MRI (age performed)	–	–	–	normal (5 years)	–	–	–	mild cerebellar atrophy (7 years)

(*Continued on next page*)

	Family 2	Family 3	Family 4		Family 5		Family 6
II-IV-7 (A2)	II-2	II-1	II-1	II-3	IV-1	IV-2	II-3
F	M	F	F	F	M	F	F
UAE	Italy	Turkey	Pakistan	Pakistan	Iran	Iran	Turkey
+	same village	+	+	+	+	+	+
3 years	16 years	15 years	13 years	2 years	died at 6 years	3 years	10 years
–	–	–	–	–	in sleep	–	–
g.36558895C>T	g.36557226C>T	g.36556868A>C	g.36557324_36557328delTGCCC	g.36557324_36557328delTGCCC	g.36557524C>T	g.36557524C>T	g.36554605G>A
c.1000C>T	c.316C>T	c.235A>C	c.414_418delTGCCC	c.414_418delTGCCC	c.530C>T	c.530C>T	c.100G>A
p.Gln334*	p.Gln106*	p.Thr79Pro	p.Ala139Glyfs*4	p.Ala139Glyfs*4	p.Ser177Leu	p.Ser177Leu	p.Asp34Asn
+	+	+	+	+	+	+	+
+	+	+	+	+	+	+	+
+	+	+	+	mild developmental delay	+	+	+
normal speech but then deteriorated	slow speech	normal	normal	delayed	normal until 1.5 years but then deteriorated with difficulty speaking	speaks only a few words	delayed
walked normally at 14 months but then had ataxia and poor balance at 19 months	normal but then deteriorated by 2 years	normal	normal but then deteriorated by 2 years	mildly delayed	normal until 1 year but then deteriorated	normal but then deteriorated by 1.5 years	normal
16 months	–	–	–	9 months	24 months	36 months	–
absence, GTCS	–	–	GTCS with illness	GTCS with illness	multifocal, GTCS	multifocal, GTCS	–
normal but then delayed	normal but then started deteriorating at age 11 yeras	normal	mild ID (IQ 60)	mild global developmental delay	normal but then stagnated	normal but then stagnated	mild ID
generalized epileptiform activity, slow background	–	–	mild slowing background activity (3 years)	normal	generalized epileptiform activity, slow background	normal	normal
mild cerebellar atrophy (7 years)	cerebellar vermis atrophy (11 years)	mild cerebellar atrophy, spinal cord atrophy (12 years)	mild cerebellar atrophy (4 years)	normal (11 months)	–	normal (3 years)	mild cerebellar vermis atrophy, spinal cord atrophy (15 years)

(*Continued on next page*)

Table 1. ***Continued***

	Family 1							
	I-IV-1	**I-IV-2**	**I-IV-3**	**I-IV-5**	**I-IV-11**	**II-IV-2**	**II-IV-5**	**II-IV-6 (A1)**
EMG or biopsy	–	–	–	–	–	–	–	nerve biopsy with severe axonal loss
Onset of unsteady gait	–	–	2.5 years	3 years	2.5 years	–	–	2.5 years
Other Clinical Features								
Exacerbated by illness and/or stress	+	+	+	+	+	+	+	+
Other clinical features	–	–	–	hypotonia with repeated pneumonia, ventilator dependent at time of death	can walk but is very unsteady	progressive weakness	progressive weakness	repeated pneumonia, repeated cardiac arrest, profound type II muscle fiber atrophy

Clinical presentation for affected subjects from families 1–6. Abbreviations are as follows: +, yes; –, not available; DTR, deep-tendon reflex; EEG, electroencephalography; EMG, electromyography; F, female; GTCS, generalized tonic-clonic seizure; ID, intellectual disability; M, male; MRI, magnetic resonance imaging; and SNHL, sensorineural hearing loss.
[a]UCSC Genome Browser.

50% decrease with the neuron-specific promoter, *elav* (*embryonic lethal abnormal visual system*) (Figure S4A). Whereas the *da*-Gal4 and $Parg^{RNAi}$ lines showed normal survival, crossing the two together led to *daughterless* (*da*)-mediated expression of $Parg^{RNAi}$, which reduced survival substantially (Figure S4B). Ubiquitous knockdown of *Parg* also led to decreased survival when animals were exposed to stress with either hydrogen peroxide (H_2O_2) in their water or environmental hypoxia (2% O_2) (Figures S4C and S4D). Furthermore, knockdown of *Parg* specifically in neurons largely recapitulated this phenotype by using the same two environmental stressors (Figures S4E and S4F). These data provide evidence that stress leads to premature death in the absence of *Parg* and that neurons play an important role in this phenotype.

However, lethality of these flies was not as severe as in the $Parg^{27.1}$ line, which carries a p-element insertion that deletes two-thirds of the open reading frame (nucelotides 34,622–36,079 of GenBank: Z98254),[14] suggesting that $Parg^{RNAi}$ is partially inactivating. These mutant flies with *Parg* loss of function lack the protein Parg and show elevated amounts of PAR, especially in nervous tissue.[14] Mutant flies die in larval stages, but 25% of the animals survive when grown at the permissive 29°C temperature. These adult flies display progressive neurodegeneration, reduced locomotion, and reduced lifespan,[14] consistent with the individuals' phenotypes in our families. We confirmed lethality of the $Parg^{27.1}$ line and found that forced expression of *Drosophila Parg* under the ubiquitous *da* promoter in the mutant background increased both survival and motor activity as measured by an established "climbing index" (Figures 3B and 3C).[20] Likewise, expression of the human *ADPRHL2* under the same *da* promoter showed a nearly identical degree of rescue of both survival and locomotor activity (Figures 3B and 3C). These results suggest that human *ADPRHL2* is a functional paralog of *Drosophila Parg*.

We next tested whether this phenotype might be ameliorated by inhibition of protein PARylation. We reasoned that the requirement for dePARylation should be reduced by the blockage of stress-induced PARylation. Minocycline displays PARP inhibitory activity with an IC_{50} of 42 nM in humans[21] and is well tolerated in flies.[22] We fed flies with a range of concentrations from 0 to 1 mg/mL minocycline for 24 hr before stress and measured survival rates 96 hr after stress induction. Drug treatment of flies with ubiquitous knockdown of *Parg* revealed a dose-dependent partial rescue of the lethality (Figure S4G). This rescue was also seen when the drug was given to flies with neuron-specific knockdown of *Parg* (Figure S4H), providing evidence that PARP inhibition can rescue lethality *in vivo*. Although we expect that the effect of minocycline on survival in this assay was due to its effect on PARP, we cannot exclude off-target or non-specific effects.[22]

Given that PARP inhibitors are currently in trials for various types of cancer, it is possible that these drugs could be tested for clinical effectiveness in this orphan disease, where they could have a positive effect. Potentially clinically relevant PARP inhibitors include (1) minocycline, an FDA-approved tetracycline derivative that displays PARP inhibitory activity; (2) dihydroisoquinoline (DPQ), a non-FDA-approved potent PARP-1 inhibitor used in experimental research; and (3) veliparib (ABT: 888), a potent PARP-1 and PARP-2 inhibitor currently in clinical trials for the treatment of various type of cancers (IC_{50} = 42, 37, and 4.4 nM, respectively).[21,23]

	Family 2	Family 3	Family 4		Family 5		Family 6
II-IV-7 (A2)	II-2	II-1	II-1	II-3	IV-1	IV-2	II-3
–	–	axonal polyneuropathy (4 years)	normal muscle biopsy (4 years)	–	normal (4 years)	axonal polyneuropathy (4 years)	axonal polyneuropathy
20 months	11 years	4 years	2.5 years	not yet	1.5 years	1.5 years	10 years
+	+	+	+	+	+	+	+
normal hearing but then developed severe SNHL, severe kyphoscoliosis, one episode of cardiac arrest	myopathic changes on muscle biopsy (11 years)	claw hand and pes cavus deformities, scoliosis, SNHL at 10 years, tracheotomy, ventilation	asthma	–	progressive weakness, tremors, frequent falling	progressive weakness, progressive external ophthalmoplegia	distal muscle atrophy, pes cavus deformity, toe abnormality, scoliosis, brisk DTRs, positive Babinski reflex, intentional tremor, ataxia

The extent to which *ADPRHL2* and *PARG* functionally diverge or converge is not well understood, partly because of a lack of detailed comparative expression analysis and biochemical function. PARG demonstrates greater specific activity than ARH3 for removing PAR from proteins,[8] and loss of *Parg* in mice is embryonically lethal.[13] Together, these data suggest that *PARG* is likely to be the major contributor to PAR removal in cells that express both genes under basal conditions. One possibility is that *ADPRHL2* acts as a backup for *PARG* to remove excessive PAR moieties under stress conditions. This would be consistent with the clinical pesentation of individuals with loss of *ADPRHL2*, where phenotypes appear to be induced by environmental stress. Recent studies have shown that ARH3 acts on a recently discovered form of Ser-ADP ribosylation.[24] For example, studies have illustrated an excessive accumulation of Ser-poly-ADP-ribosylated enzymes in *ADPRHL2*$^{-/-}$ cell lines and that ARH3 acts mainly on

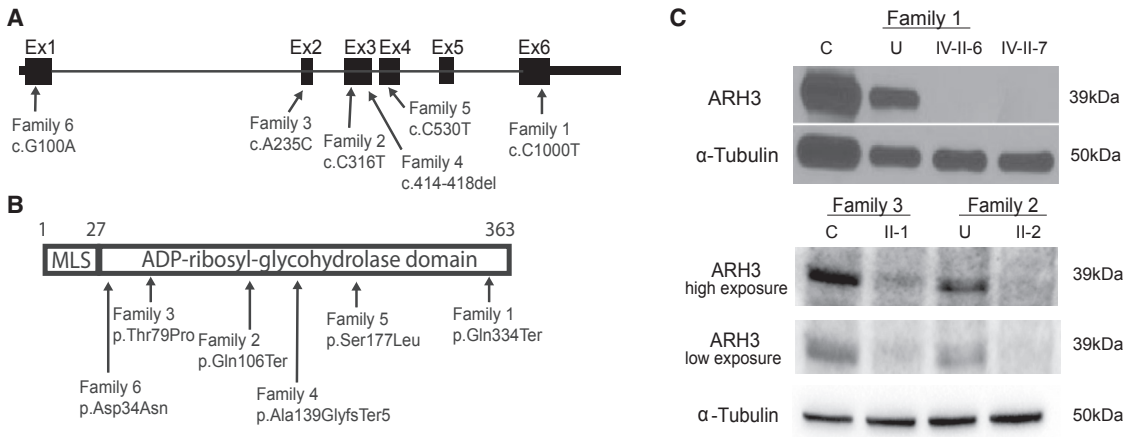

Figure 2. Truncating and Missense *ADPRHL2* Mutations in Six Independent Families Are Predicted to Be Inactivating
(A) Schematic of *ADPRHL2* depicts the coding sequence spanning six exons and the 5′ and 3′ UTRs. Black arrows indicate the positions of the six identified mutations and their coordinates within the cDNA (Gene ID: 54936).
(B) Schematic of ARH3 depicts the mitochondrial localization sequence (MLS) and the ADP-ribosyl-glycohydrolase domain. Black arrows indicate the position and coordinates of the impact of the described mutations.
(C) Western blot of fibroblasts from an unrelated control individual (C), the unaffected carrier father (U), and affected individuals IV-II-6 and IV-II-7 from family 1 shows the absence of ARH3 in affected fibroblasts. α-tubulin was used as the loading control. Western blot of fibroblasts from an unrelated control individual (C) and affected individual II-1 from family 3 and the unaffected carrier mother (U) and affected individual II-3 from family 2 shows significantly reduced amounts of ARH3. α-tubulin was used as the loading control.

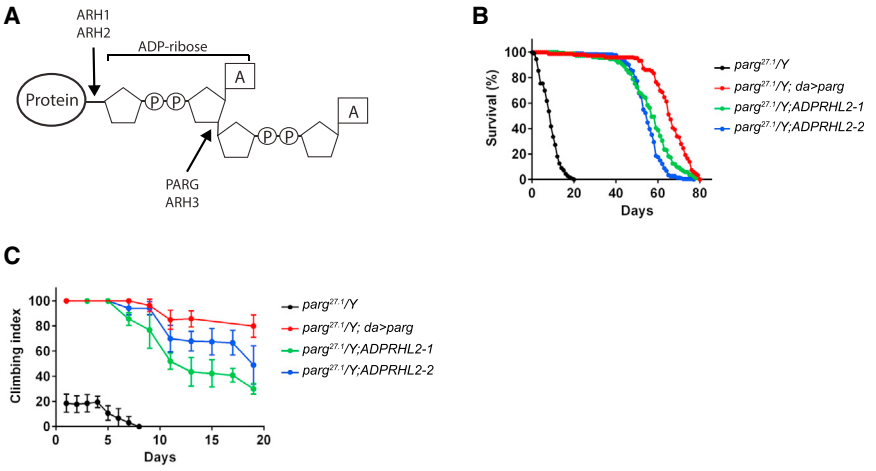

Figure 3. Premature Death and Locomotor Defects in *Drosophila Parg* Mutants Are Rescued by Human *ADPRHL2*

(A) Schematic of a poly-ADP-ribosylated protein and the location of cleavage. *PARG* and *ADPRHL2* both remove poly-ADP-ribose (PAR) from proteins and cleave the same site. *Drosophila melanogaster* has one PAR-removing enzyme, Parg.

(B) $Parg^{27.1}$ mutant flies (black) show a severe climbing defect, which was rescued by ubiquitous forced expression of *Parg* (red) or mis-expression of human *ADPRHL2* in two different transgenic lines (green and blue).

(C) $Parg^{27.1}$ mutant flies (black) displayed decreased survival, which was rescued with ubiquitous forced expression of *Parg* (red) and two different transgenic lines expressing human *ADPRHL2* (green and blue). Data represent the mean ± SEM of eight experiments.

Ser-ADPr removal.[25] This would be consistent with the phenotype we see in subjects with loss of ARH3, where phenotypes do not emerge until environmental stress insults are encountered. Finally, ARH3 contains a mitochondrial localization signal, and thus another possibility is that ARH3 functions as a mitochondrial-specific glycohydrolase that is required after the induction of oxidative stress.[13]

PAR signaling has been shown to play a role in a number of cellular processes—including the regulation of transcription, telomere function, mitotic spindle formation, intracellular trafficking, and energy metabolism—in addition to apoptosis-inducing-factor (AIF)-mediated apoptosis.[2,3] Although we hypothesize that the disease mechanism is through cell death, it is possible that PAR accumulation could affect other cellular processes before this. Further work is needed to characterize these effects in the context of this disease.

Accession Numbers

The exome sequencing data from individuals from the University of California, San Diego, study site have been deposited in the Database of Genotypes and Phenotypes under accession number dbGaP: phs000288.v1.

Supplemental Data

Supplemental Data include a Supplemental Note, Supplemental Material and Methods, four figures, and one table and can be found with this article online at https://doi.org/10.1016/j.ajhg.2018.07.010.

Acknowledgments

The authors thank the subjects and their families for participating in this study. S.G. was sponsored by the Ruth L. Kirschstein Institutional National Research Service Award (T32 GM008666) from the National Institute on Deafness and Other Communication Disorders and by award F31HD095602 from the NIH Eunice Kennedy Shriver National Institute of Child Health and Human Development. We thank the Broad Institute (U54HG003067 to E. Lander and UM1HG008900 to D. MacArthur) and the Yale Center for Mendelian Disorders (U54HG006504 to R. Lifton and M. Gunel). We also thank Lisa Weixler for technical assistance and all the staff of the Cologne Center for Genomics for next-generation sequencing. The sequencing data were analyzed with the CHEOPS high-performace computer cluster of the Regional Computing Center of the University of Cologne. We thank DeCode for whole-genome sequencing. This work was supported by NIH grants R01NS048453 and R01NS052455, the Simons Foundation Autism Research Initiative, the Howard Hughes Medical Institute (to J.G.G.), the Deutsche Forschungsgemeinschaft Emmy Noether Programme (grant CI 218/1-1 to S.C.), the Wellcome Trust (WT093205MA and WT104033AIA), Ataxia UK, the UCL/UCLH NIHR Biomedical Research Centre, the Medical Research Council (to H.H. and M.H), EU Horizon 2020 Solve-RD, and the European Community's Seventh Framework Programme (FP7/2007-2013) under grant 2012-305121 for the "Integrated European -omics research project for diagnosis and therapy in rare neuromuscular and neurodegenerative diseases (NEUROMICS)" to B.W.

Declaration of Interests

The authors declare no competing interests.

Received: April 16, 2018
Accepted: July 15, 2018
Published: August 9, 2018

Web Resources

1000 Genomes, http://browser.1000genomes.org
dbSNP, http://www.ncbi.nlm.nih.gov/projects/SNP
Exome Aggregation Consortium (ExAC) Browser, http://exac.broadinstitute.org/
dbGaP, https://www.ncbi.nlm.nih.gov/gap
FlyBase, http://flybase.org

GenBank, https://www.ncbi.nlm.nih.gov/genbank/
Gene, https://www.ncbi.nlm.nih.gov/gene
GeneMatcher, https://genematcher.org
HaplotypeCaller and GATK, https://www.broadinstitute.org/gatk/
Iranome, http://www.iranome.ir/
Mutation Assessor, http://mutationassessor.org/
MutationTaster, http://mutationtaster.org/
NHLBI Exome Sequencing Project Exome Variant Server, http://evs.gs.washington.edu/EVS/
OMIM, http://omim.org/
PolyPhen-2, http://genetics.bwh.harvard.edu/pph2/
Provean, http://provean.jcvi.org
RefSeq, http://www.ncbi.nlm.nih.gov/RefSeq
SIFT, http://sift.jcvi.org/
UniProt, http://www.uniprot.org

References

1. Hassa, P.O., Haenni, S.S., Elser, M., and Hottiger, M.O. (2006). Nuclear ADP-ribosylation reactions in mammalian cells: Where are we today and where are we going? Microbiol. Mol. Biol. Rev. *70*, 789–829.
2. Luo, X., and Kraus, W.L. (2012). On PAR with PARP: Cellular stress signaling through poly(ADP-ribose) and PARP-1. Genes Dev. *26*, 417–432.
3. Schreiber, V., Dantzer, F., Ame, J.C., and de Murcia, G. (2006). Poly(ADP-ribose): Novel functions for an old molecule. Nat. Rev. Mol. Cell Biol. *7*, 517–528.
4. De Vos, M., Schreiber, V., and Dantzer, F. (2012). The diverse roles and clinical relevance of PARPs in DNA damage repair: Current state of the art. Biochem. Pharmacol. *84*, 137–146.
5. Wang, Z., Wang, F., Tang, T., and Guo, C. (2012). The role of PARP1 in the DNA damage response and its application in tumor therapy. Front. Med. *6*, 156–164.
6. Andrabi, S.A., Kim, N.S., Yu, S.W., Wang, H., Koh, D.W., Sasaki, M., Klaus, J.A., Otsuka, T., Zhang, Z., Koehler, R.C., et al. (2006). Poly(ADP-ribose) (PAR) polymer is a death signal. Proc. Natl. Acad. Sci. USA *103*, 18308–18313.
7. Wang, Y., Dawson, V.L., and Dawson, T.M. (2009). Poly(ADP-ribose) signals to mitochondrial AIF: A key event in parthanatos. Exp. Neurol. *218*, 193–202.
8. Oka, S., Kato, J., and Moss, J. (2006). Identification and characterization of a mammalian 39-kDa poly(ADP-ribose) glycohydrolase. J. Biol. Chem. *281*, 705–713.
9. Poitras, M.F., Koh, D.W., Yu, S.W., Andrabi, S.A., Mandir, A.S., Poirier, G.G., Dawson, V.L., and Dawson, T.M. (2007). Spatial and functional relationship between poly(ADP-ribose) polymerase-1 and poly(ADP-ribose) glycohydrolase in the brain. Neuroscience *148*, 198–211.
10. Magdaleno, S., Jensen, P., Brumwell, C.L., Seal, A., Lehman, K., Asbury, A., Cheung, T., Cornelius, T., Batten, D.M., Eden, C., et al. (2006). BGEM: An in situ hybridization database of gene expression in the embryonic and adult mouse nervous system. PLoS Biol. *4*, e86.
11. Koh, D.W., Lawler, A.M., Poitras, M.F., Sasaki, M., Wattler, S., Nehls, M.C., Stöger, T., Poirier, G.G., Dawson, V.L., and Dawson, T.M. (2004). Failure to degrade poly(ADP-ribose) causes increased sensitivity to cytotoxicity and early embryonic lethality. Proc. Natl. Acad. Sci. USA *101*, 17699–17704.
12. Niere, M., Kernstock, S., Koch-Nolte, F., and Ziegler, M. (2008). Functional localization of two poly(ADP-ribose)-degrading enzymes to the mitochondrial matrix. Mol. Cell. Biol. *28*, 814–824.
13. Niere, M., Mashimo, M., Agledal, L., Dölle, C., Kasamatsu, A., Kato, J., Moss, J., and Ziegler, M. (2012). ADP-ribosylhydrolase 3 (ARH3), not poly(ADP-ribose) glycohydrolase (PARG) isoforms, is responsible for degradation of mitochondrial matrix-associated poly(ADP-ribose). J. Biol. Chem. *287*, 16088–16102.
14. Hanai, S., Kanai, M., Ohashi, S., Okamoto, K., Yamada, M., Takahashi, H., and Miwa, M. (2004). Loss of poly(ADP-ribose) glycohydrolase causes progressive neurodegeneration in *Drosophila melanogaster*. Proc. Natl. Acad. Sci. USA *101*, 82–86.
15. Bütepage, M., Eckei, L., Verheugd, P., and Lüscher, B. (2015). Intracellular mono-ADP- ribosylation in signaling and disease. Cells *4*, 569–595.
16. Hoch, N.C., Hanzlikova, H., Rulten, S.L., Tétreault, M., Komulainen, E., Ju, L., Hornyak, P., Zeng, Z., Gittens, W., Rey, S.A., et al.; Care4Rare Canada Consortium (2017). XRCC1 mutation is associated with PARP1 hyperactivation and cerebellar ataxia. Nature *541*, 87–91.
17. Sobreira, N., Schiettecatte, F., Valle, D., and Hamosh, A. (2015). GeneMatcher: A matching tool for connecting investigators with an interest in the same gene. Hum. Mutat. *36*, 928–930.
18. Schwarz, J.M., Rödelsperger, C., Schuelke, M., and Seelow, D. (2010). MutationTaster evaluates disease-causing potential of sequence alterations. Nat. Methods *7*, 575–576.
19. Mueller-Dieckmann, C., Kernstock, S., Lisurek, M., von Kries, J.P., Haag, F., Weiss, M.S., and Koch-Nolte, F. (2006). The structure of human ADP-ribosylhydrolase 3 (ARH3) provides insights into the reversibility of protein ADP-ribosylation. Proc. Natl. Acad. Sci. USA *103*, 15026–15031.
20. Madabattula, S.T., Strautman, J.C., Bysice, A.M., O'Sullivan, J.A., Androschuk, A., Rosenfelt, C., Doucet, K., Rouleau, G., and Bolduc, F. (2015). Quantitative analysis of climbing defects in a *Drosophila* model of neurodegenerative disorders. J. Vis. Exp. *100*, e52741.
21. Alano, C.C., Kauppinen, T.M., Valls, A.V., and Swanson, R.A. (2006). Minocycline inhibits poly(ADP-ribose) polymerase-1 at nanomolar concentrations. Proc. Natl. Acad. Sci. USA *103*, 9685–9690.
22. Lee, G.J., Lim, J.J., and Hyun, S. (2017). Minocycline treatment increases resistance to oxidative stress and extends lifespan in *Drosophila* via FOXO. Oncotarget *8*, 87878–87890.
23. Donawho, C.K., Luo, Y., Luo, Y., Penning, T.D., Bauch, J.L., Bouska, J.J., Bontcheva-Diaz, V.D., Cox, B.F., DeWeese, T.L., Dillehay, L.E., et al. (2007). ABT-888, an orally active poly(-ADP-ribose) polymerase inhibitor that potentiates DNA-damaging agents in preclinical tumor models. Clin. Cancer Res. *13*, 2728–2737.
24. Fontana, P., Bonfiglio, J.J., Palazzo, L., Bartlett, E., Matic, I., and Ahel, I. (2017). Serine ADP-ribosylation reversal by the hydrolase ARH3. eLife *6*, e28533.
25. Palazzo, L., Leidecker, O., Prokhorova, E., Dauben, H., Matic, I., and Ahel, I. (2018). Serine is the major residue for ADP-ribosylation upon DNA damage. eLife *7*, e34334.

The American Journal of Human Genetics, Volume *103*

Supplemental Data

Biallelic Mutations in *ADPRHL2*, Encoding ADP-Ribosylhydrolase 3, Lead to a Degenerative Pediatric Stress-Induced Epileptic Ataxia Syndrome

Shereen G. Ghosh, Kerstin Becker, He Huang, Tracy D. Salazar, Guoliang Chai, Vincenzo Salpietro, Lihadh Al-Gazali, Quinten Waisfisz, Haicui Wang, Keith K. Vaux, Valentina Stanley, Andreea Manole, Ugur Akpulat, Marjan M. Weiss, Stephanie Efthymiou, Michael G. Hanna, Carlo Minetti, Pasquale Striano, Livia Pisciotta, Elisa De Grandis, Janine Altmüller, Peter Nürnberg, Holger Thiele, Uluc Yis, Tuncay Derya Okur, Ayse Ipek Polat, Nafise Amiri, Mohammad Doosti, Ehsan Ghayoor Karimani, Mehran B. Toosi, Gabriel Haddad, Mert Karakaya, Brunhilde Wirth, Johanna M. van Hagen, Nicole I. Wolf, Reza Maroofian, Henry Houlden, Sebahattin Cirak, and Joseph G. Gleeson

Supplemental Data

Supplemental Note: Case Reports

Family 1 is from the United Arab Emirates (UAE), with 9 affected individuals in two branches, matching a recessive mode of inheritance. In this family, two brothers married two sisters that were both first cousins. All affected family members had normal pregnancy, labor, delivery, unremarkable newborn periods, and displayed typical developmental milestones. All affected individuals developed seizures between the ages of 1-2 years of age. The diagnosis of epilepsy predated developmental stagnation and loss of milestones. In some children, the presentation was consistent with sudden unexplained death in epilepsy (SUDEP, MIM: 617116). The connection with SUDEP was intriguing, and not well medically documented, but parents of both branches report that four of the children were healthy, then found dead during routine activities such as eating cereal, playing on a swing-set, or sleeping. The clinical presentation of this family did not match any reported conditions in the medical literature, and the physicians were not able to abate the clinical features with medical therapy.

Individual II-IV-6 was born full-term without complications. At 13 months, following a typical upper respiratory infection, he developed brief, absence-like episodes, which persisted weekly thereafter, mostly upon waking and without loss of consciousness. At 14 months he developed episodes that began with sudden stiffening of the back, followed by head deviation and loss of consciousness. These occurred 1-3 times per day, were diagnosed as generalized tonic-clonic seizures, and were refractory to antiepileptic treatment. At age 2 years, he showed signs of speech and developmental delay. MRI of the brain showed possible periventricular white matter loss but was otherwise structurally normal. EEG, EKG, karyotype, serum amino acids, lactate, pyruvate, and urine organic acids to evaluate for mitochondrial dysfunction were normal

repeatedly. At age 5 years, he was able to walk but his gait was unsteady and he suffered relapsing-remitting upper respiratory infection-associated cyclic episodes of depressed consciousness and hypoventilation requiring intubation, which each time was associated with further loss of developmental milestones. Muscle and nerve biopsies showed profound Type II fiber atrophy with severe axonal loss. The subject could not wean from the ventilator, requiring a tracheostomy and gastrostomy tube for life support. Following the resolution of an acute illness with supportive therapy, his condition improved slowly and some previous skills returned, but this was quickly followed by further illness and loss of milestones. He had a series of cardiac arrests during acute exacerbations, but recovered with aggressive resuscitation. At age 9 years, MRI showed cerebral volume loss, amygdala and hippocampal atrophy (Fig. 1B). MR spectroscopy showed elevated N-acetyl aspartate in white matter voxels, suggesting ongoing neuronal degeneration. EEG showed frontal intermittent rhythmic delta activity and lack of clear posterior dominant rhythm, supporting white matter involvement. He did not improve significantly with physiotherapy and after a prolonged medically related transcontinental air flight, he died of respiratory failure at age 9. The clinical course for his sibling (II-IV-7) was similar to the index case except that she, with previously normal hearing, developed severe sensorineural hearing loss and paralysis of the right diaphragm during the course of her disease. MRI of the brain also showed possible periventricular white matter loss and enlarged ventricles, but was otherwise structurally normal. Repeated mitochondrial studies revealed no accumulation of relevant intermediates, and she remains in stable condition.

Family 2 is from Sicily with one affected individual, who is currently 16 years old. This boy is the second of two children born from healthy Sicilian parents, who report no consanguinity (but are from the same village) and who have no history of neurological disorders. His growth parameters at birth were within normal range and the parents

report no concerns in the neonatal or early infantile age. Since the age of 10 years, he began experiencing balance difficulties and by age 11, showed gait abnormalities with progressive ataxia. Also at that time, abnormal ophthalmological features including nystagmus diplopia were noticed. His speech development was normal; however, his intellectual ability began to decline. At age 11, visually evoked potentials showed irregular waveform and amplitude within low limits. At the same time, the boy started to present cognitive difficulties and behavior abnormalities.

As part of the diagnostic work-up to define his condition, extensive metabolic and genetic investigations (including ataxia genes panel sequencing) were performed and fully reported as normal. Brain MRI performed at the age of 11 years showed cerebellar vermis hypoplasia/atrophy. There were some non-specific myopathic changes on his muscle biopsy. Peripheral nerve conductions studies showed low compound muscle action potentials (CMAPs) and axonal neuropathy. He developed ophthalmological features including nystagmus and diplopia. He also has severe scoliosis. Since the age of 10 years, he started to experience balance difficulties and since the age of 11, showed gait abnormalities with progressive ataxia. At the age of 14 years, there was a worsening of ataxia with severe difficulties in walking autonomously. He developed gynecomastia at the age of 10 years and endocrinological tests showed mild hypogonadism with elevated FSH values. Additionally, during the disease course, he experienced several episodes of hyperthermia, not responsive to paracetamol treatment, especially during the summer season. On last neurological examination at age of 15 years deep tendon reflexes were reduced. Cerebellar tests were impaired and he showed dysmetria. Tongue fasciculations were also noticed.

Family 3 is a Turkish family with one affected child born to consanguineous parents. She had normal developmental milestones. At the age of 4 years, she began to develop weakness in her upper and lower extremities and had difficulties in walking and

abnormal gait. Cognitive functions remained initially normal. Her older brother had been diagnosed with cerebral palsy and died at the age of 9 years but further investigations have not been performed. Examinations at the age 8 years in another hospital revealed a mixed type polyneuropathy and sensorineural hearing loss, with normal brain and spine MRI. Since a chronic inflammatory polyneuropathy was suspected, an intravenous immunoglobulin treatment was started. However, there was no clinical benefit and she became wheelchair-dependent at the age of 12 years old.

Physical examination at the age of 12 years revealed symmetric muscle atrophy in upper and lower extremities. Muscle power was 4/5 and 3/5 in proximal and distal muscles of upper and lower extremities, respectively. There was thenar and hypothenar atrophy, claw hand and pes cavus deformities. Deep tendon reflexes were absent. Abduction of the eyes were restricted bilaterally. There were tongue fasciculations. Cerebellar tests were mildly impaired and speech was dysarthric. Brain MRI showed mild cerebellar atrophy. There were no dysmorphic features and mental functions were normal.

All metabolic investigations including serum and urinary amino acids, urinary organic acids, TANDEM analysis, very long chain fatty acids, serum biotidinase, serum ammonia, lactate and pyruvate were normal. Brain and spinal MRI showed mild cerebellar and spinal cord atrophy. On electroneuromyography, sensory responses were absent and only left median nerve could be stimulated. Nerve conduction of left median nerve was reduced (34.4 m/s) and amplitudes were very low (wrist: 390 μV and elbow: 328 μV). Needle electromyography showed polyphasic potentials. Repeated hearing test revealed moderate sensorineural hearing loss on the left and severe sensorineural hearing loss on the right.

Genetic analysis for *PMP22, SCA 1 and 2* were normal. Progressive hearing loss, axonal polyneuropathy and worsening of respiratory functions during infections

suggested riboflavin responsive neuropathy, and co-enzyme Q10 (100 mg/day) and riboflavin (200 mg/day) were started. However, she did not benefit and weakness worsened. She became home-ventilator-dependent with tracheostomy. Mental function remained normal but she became bed ridden.

Family 4 originated from Pakistan, and parents were first cousins. Their first daughter was born after pregnancy complicated by gestational diabetes. Delivery and early development were normal. The subject was able to walk without support around age 18 months. She was diagnosed with asthma. At the age of two years, parents noted that gait became more unstable, with swaying of arms to keep her balance. During varicella infection, this deteriorated, and she was almost no longer able to sit and had a head tremor. Neurological examination at age 3.5 years showed mild dysarthria, a cerebellar eye movement disorder with saccadic pursuit and hypometric saccades, evident gait ataxia and mild intention tremor and dysmetria. In addition, muscle tendon reflexes were exaggerated at the legs, with bilateral Babinski signs. Funduscopy was normal. General pediatric exam was normal. MRI was initially normal. At the age of 4.5 years, she had mild cerebellar atrophy, which remained stable. Extensive metabolic investigations (plasma, urine and CSF) were normal except a slightly positive filipin test in fibroblasts, which led to the suspicion of Niemann-Pick type C disease. NPC1 and NPC2 were sequenced, but no explanation found. Muscle biopsy revealed non-specific mild atrophy of type 2 fibers and variation in fiber diameter; respiratory chain function in fresh tissue was normal as well as mitochondrial morphology. Whole-exome sequencing in 2015 was initiated. Clinical course during the last 10 years remained remarkably stable (with the exception of deterioration with viral infections), and the subject was able to walk without support at age 13 years with mild mental retardation. Neurological examination showed spastic ataxia. Parents conveyed that high temperatures led to deterioration of symptoms. The youngest sister of the index individual was born after a pregnancy

complicated by gestational diabetes, without complications. Early development was slow. She presented with generalized tonic-clonic seizures at age 9 months responding well to monotherapy with valproic acid. At age 2 years, she had mild global developmental delay, walked without support age at 18 months, spoke several words and some two-word combinations at age 23 months. Neurological examination at age 23 months was normal. Brain MRI as well as metabolic testing of plasma, urine and CSF was entirely normal, and whole-genome sequencing was initiated. This analysis revealed the same homozygous variant in *ADPRHL2* in both sisters, in addition to a *de novo* mutation in *CSNK2B* (OMIM: 115441, c.T161A p.Leu54Ter) in the youngest sister.

Family 5 was from Iran with 2 affected individuals, whose parents are first cousins. The proband (II-2) displayed normal developmental milestones until 18 months of age when she regressed significantly. She was noted to have muscle weakness and ataxic gaits. She began having epileptic attacks, which were controlled with phenobarbital; however, EEG and metabolic testing were normal. MRI performed at the age of 3 years showed abnormal white matter signal intensity in the bioccipital lobe but was otherwise structurally normal. EMG performed at the age of 3 years old indicated chronic sensorimotor distal polyneuropathy with axonal features. There were multiple oculomotor features including nystagmus, strabismus in one eye, putative external ophthalmoplegia with ptosis, impaired saccades, and upward gaze, suggesting brainstem dysfunction. She has recently started to walk with the help of her parents and she speaks only a few words and she has autistic features. Her affected brother (II-1) exhibited similar presentation, with onset of symptoms around 18 months of age with frequent falling, hypotonia, muscle weakness, tremor and seizure controlled by valproate. Neurological examination at the age of 4 years showed that he was developmentally normal with normal cognition but the DTR are decreased. MRI taken at the age of 3 years old showed mild cerebellar atrophy. He was able to walk with difficulty. EMG and NCV at the

age of 4 years old were normal. He also developed ataxia, poor balance and autistic features. He passed away at the age of 6 years old suddenly during sleep with no known cause.

Family 6 is a Turkish family with one affected female individual II-3 who is at the age of 16 years. She was born at term from healthy consanguineous parents after an uneventful pregnancy and delivery. She had two siblings. One of them died at the age of 18 years because of Wilson disease complications. The diagnosis of Wilson was confirmed pathologically. The other sibling was never able to walk independently and was first seen at the age of 11 months in another clinic because of motor delay and dropped head. His mental functions were normal but he developed severe scoliosis and distal muscle weakness and atrophy. He died suddenly due to SUDEP during the course of an upper respiratory tract infection.

Case II-3 was admitted to the neonatal intensive care unit for one week because of feeding difficulties and vomiting. She was later discharged and reached her motor milestones at normal ages. However, she had speech delay and started to talk at the age of 3 years. By the age of 13 years, she began to show gait abnormalities with difficulties in walking. She was admitted to a pediatric neurology clinic with the complaints of severe fatigue and progressive weakness.

On physical examination, she was in an apathic mood. Her upper extremity muscle strength was 4/5, lower extremity muscle strength was 3/5. Distal muscle groups were more affected than proximal muscle groups. She had symmetrical atrophy in intrinsic hand and peroneal muscles. Deep tendon reflexes were increased and the Babinski sign was bilaterally positive. She also had a scoliosis and showed pes cavus deformities. Cerebellar examination revealed head titubation, mild intention tremor, head tremor and dysarthric speech. Her proprioception was also impaired and the Romberg sign with closed eyes was positive. WISC-R test performed at 15 years of age showed mild

intellectual disability. The disease progressed to permanent muscular weakness of distal lower and upper extremities and she became wheelchair dependent at the age of 15.

Laboratory studies including complete blood cell count, infectious and metabolic evaluations revealed no abnormalities. Creatine kinase levels were slightly elevated ranging from 230 to 435 U/L (normal values: 0-145 U/L). Brain and spinal MRI performed at the age of 15 years showed mild cerebellar vermis atrophy and spinal cord atrophy. Ophthalmological examination, electroencephalography and auditory brainstem response (ABR) tests were normal. Nerve conduction studies revealed mild conduction delay in the right median nerve (40 m/sec) and the right tibial nerve (35 m/sec). Sural sensory responses could not be obtained. Peroneal nerves could not be stimulated. Compound muscle action potentials of right median and ulnar nerves were normal but compound muscle action potentials of tibial nerve were severely reduced (proximal: 330 μv, distal: 249 μv). Needle electromyography examinations at rest showed fibrillations and positive waves in tibialis anterior muscles consistent with severe denervation. Results were compatible with lower limb dominant axonal sensorimotor polyneuropathy.

Supplemental Figures and Tables

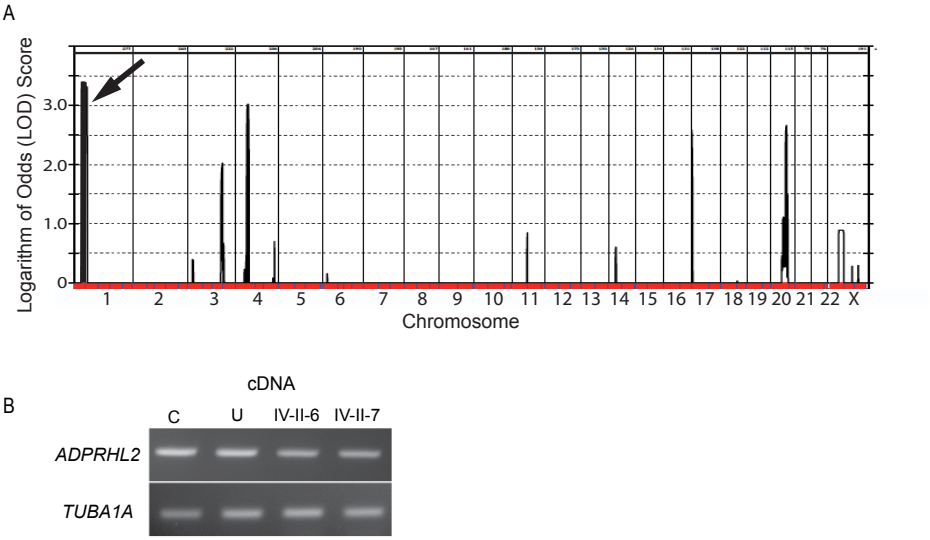

Figure S1. Linkage analysis and RT-PCR for family 1.

(A) Multipoint linkage plot for the family shows a peak on chromosome 1 with a maximum LOD score of 3.4 (arrow) and lower peaks on chromosomes 4 and 20.

(B) RT-PCR results of fibroblasts from unrelated control (C), unaffected carrier Father (U), and affected individuals (IV-II-6 and IV-II-7) from Family 1 shows normal *ADPRHL2* mRNA levels.

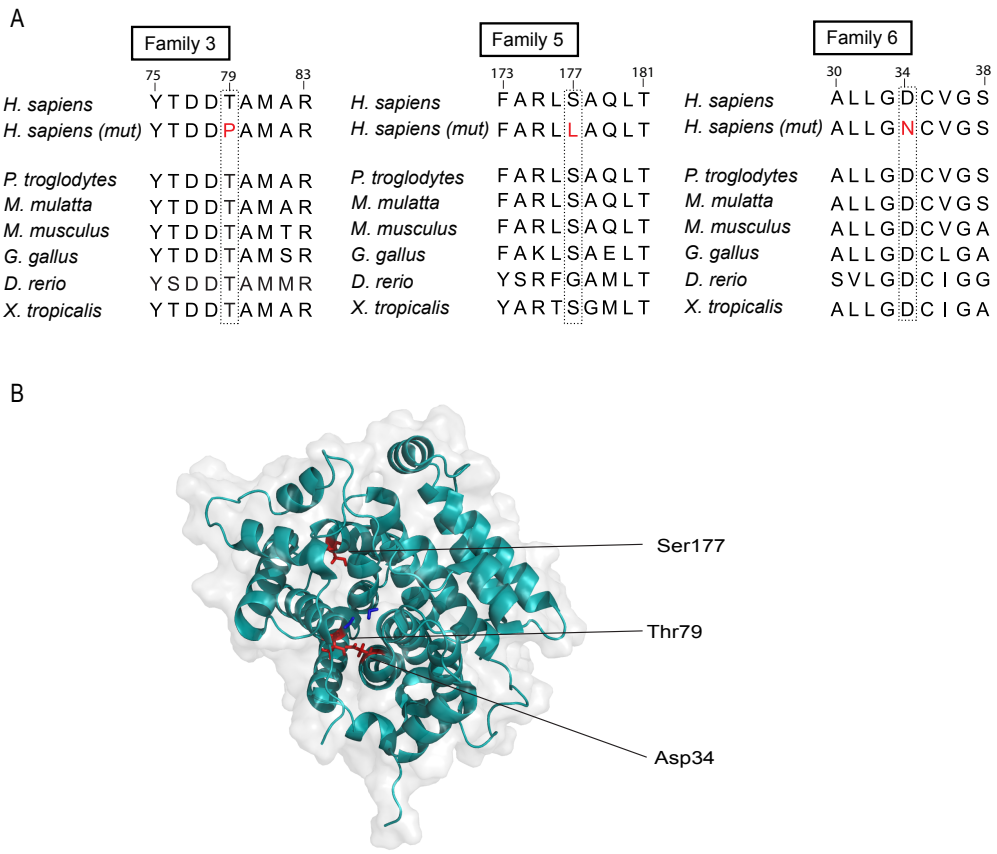

Figure S2. Families 3, 5 and 6 carry *ADPRHL2* missense mutations that affect conserved amino acid residues.

(A) The amino acid missense mutations in Families 3, 5, and 6 are conserved in almost all vertebrates.

(B) Cartoon model of *ADPRHL2* as solved at 1.6 Angstrom resolution.[7] Depicted are the mutated residues, Ser177, Thr79, and Asp34 in red within alpha-helical domains. Mg^{2+} ions are shown in blue.

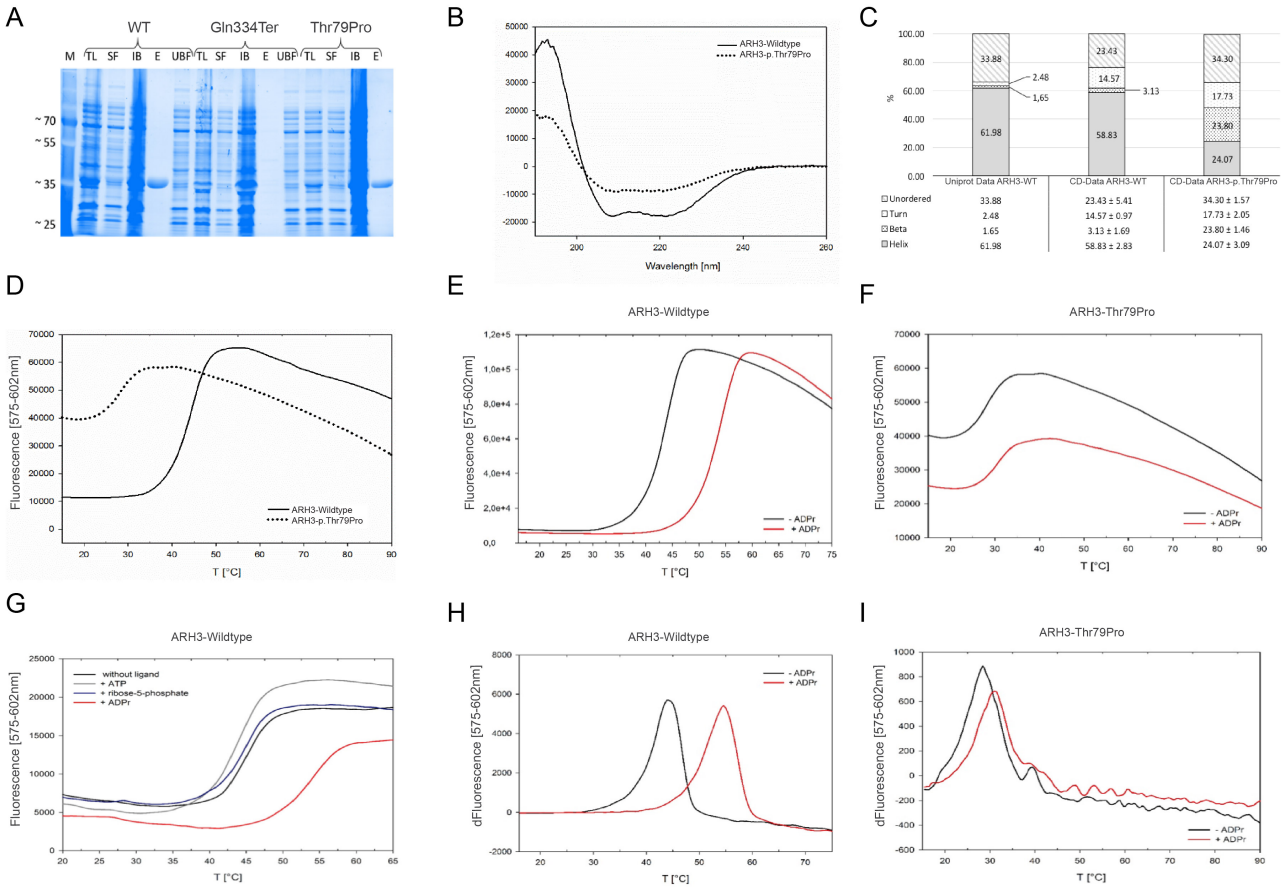

Figure S3. Biochemical characterization of Wildtype ARH3 and mutants on protein stability and substrate binding.

(A) Recombinant protein purification of ARH3 Wildtype (WT) and mutants with His-tag affinity chromatography. TL: total lysate, SF: soluble fraction, IB: inclusion body, E: elution of pure proteins, UBF: unbound flow through.

(B-C) CD-spectroscopy measurement of secondary structure of ARH3-Wildtype and mutants. (B) Normalized exemplary presentation of the CD-spectra of recombinant ARH3-Wildtype and ARH3-p.Thr79Pro. Molar ellipticity [θ] measured at 10°C in a range of 190-260 nm. (C) Experimentally determined composition of the secondary structural elements of ARH3-Wildtype and ARH3-p.Thr79Pro. Comparison of Uniprot data and CD-derived data from ARH3-Wildtype and ARH3-p.Thr79Pro. The data analysis was carried out with DichroWeb and is based on the algorithm CONTINLL.[10,11] The mean values and standard deviation of the CD-data analysis are tabulated in percent. ARH3-

Wildtype n=3 NRMSD >0.05; ARH3-p.T79P n=3 NRMSD >0.08. (NRMSD= Normalized root-mean-square deviation).

(D-I) Thermal stabilities of ARH3-Wildtype and ARH3-Thr79Pro measured via the thermofluor assay. Measured using 6 µg protein, ROX filter (575-602nm) and SYPRO orange dye. (D) Thermofluor melt curves of recombinant ARH3-Wildtype and ARH3-p.Thr79Pro. Average melting temperatures: ARH3-Wildtype= 44.79 °C; ARH3-p.Thr79Pro= 28.37 °C. (E) Thermofluor melt curves of recombinant ARH3-Wildtype with different ligands (100 µM). Average melting temperatures: ARH3-Wildtype= 45.74 °C; ARH3-Wildtype+ ATP=44.57°C; ARH3-Wildtype+ribose-5-phosphate=45.75 °C; ARH3-Wildtype+ADPr= 54.52°C. (F) Normalized and (G) derivative ARH3-Wildtype melt curve in the presence of adenosine diphosphate ribose (ADPr). Average melting temperatures: ARH3-Wildtype= 43.87 °C; ARH3-Wildtype+ADPr= 54.59 °C. (H) Normalized and (I) derivative ARH3-p.Thr79Pro melt curve. Average melting temperatures: ARH3-p.Thr79Pro= 28.37 °C; ARH3-p.Thr79Pro + ADPr= 31.05 °C.

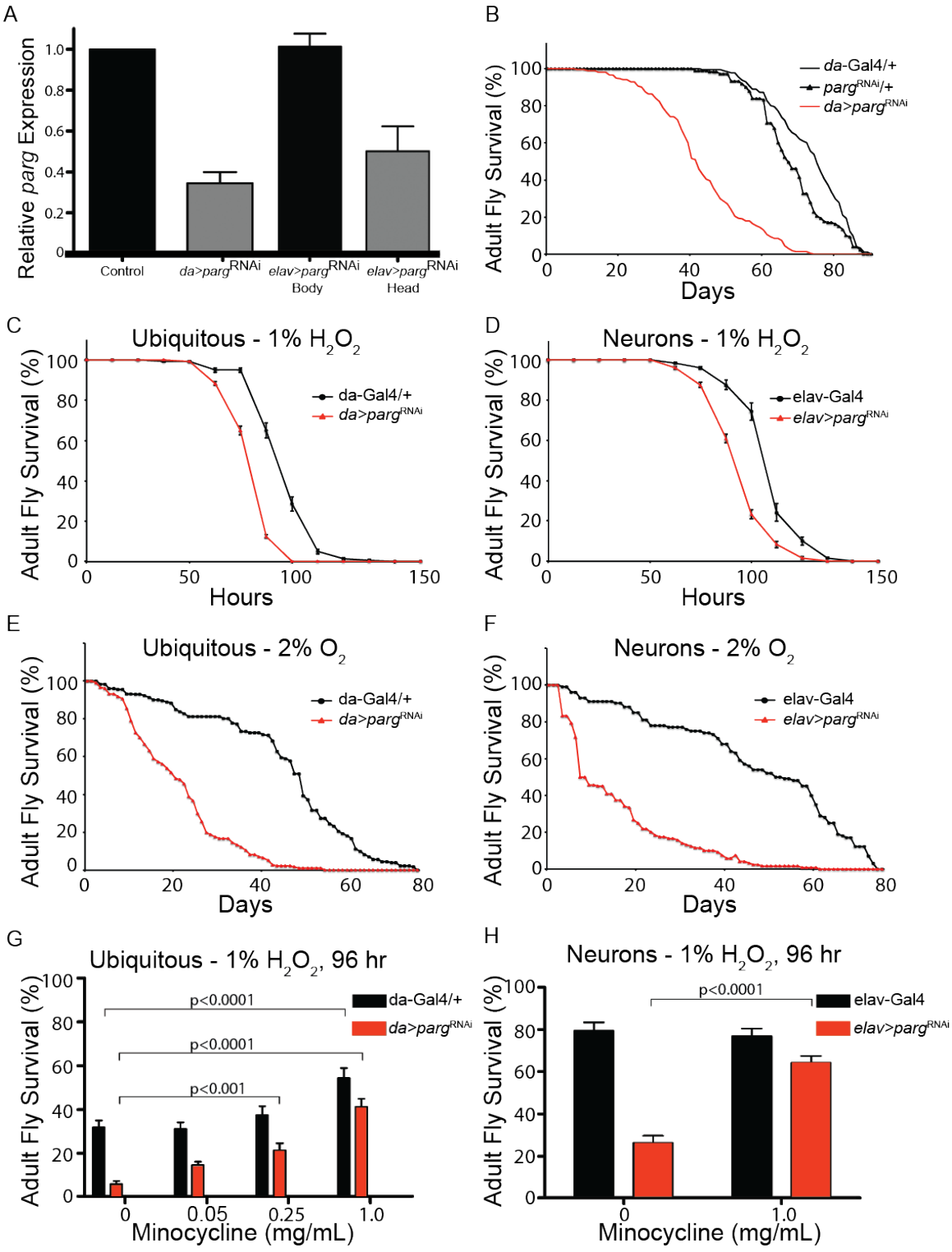

Figure S4. *Drosophila mutants* display increased survival with PARP inhibition. (A) Relative *parg* expression in ubiquitous knockdown animals under the *daughterless (da)* promoter shows that RNAi leads to an ~60% in *parg* mRNA levels. Relative *parg*

expression in neuron-specific knockdown animals under the *elav* promoter shows that RNAi leads to an ~50% in *parg* mRNA levels in the head of the animal only.
(B) Mutant flies with a ubiquitous decrease in *parg* by RNAi die prematurely (red) compared with parental stocks (black).
(C,E) Flies with ubiquitous knockdown of *parg* under the *daughterless (da)* promoter display decreased survival when exposed to oxidative stress or low oxygen.
(D,F) Flies with knockdown of *parg* under the neural *elav* promoter display decreased survival when exposed to oxidative stress or low oxygen.
(G,H) Flies with ubiquitous and neuronal knockdown of *parg* can show increased survival in the presence of hydrogen peroxide when pre-treated with Minocycline. Kaplan–Meier Log-rank Test. Data is mean ± s.e.m. of n=8 experiments.

Table S1. Detailed information for all mutations detected in affected individuals from families 1-6, including gene name, transcript number, genetic (gDNA) and complementary DNA (cDNA) position, and protein position.

Family	Gene	Transcript	gDNA pos.	cDNA pos.	Protein pos.
Family 1	*ADPRHL2*	NM_017825.2	g.36558895C>T	C.1000C>T	p.Gln334Ter
Family 2	*ADPRHL2*	NM_017825.2	g.36557226C>T	c.316C>T	p.Gln106Ter
Family 3	*ADPRHL2*	NM_017825.2	g.36556868A>C	c.235A>C	p.Thr79Pro
Family 4	*ADPRHL2*	NM_017825.2	g.36557324_36557328delTGCCC	c.414_418delTGCCC	p.Ala139Glyfs*4
Family 5	*ADPRHL2*	NM_017825.2	g.36557524C>T	c.530C>T	p.Ser177Leu
Family 6	*ADPRHL2*	NM_017825.2	g. 36554605G>A	c.100G>A	p.Asp34Asn

Supplemental Materials and Methods

Linkage Analysis and Exome Sequencing

This study was approved by the Institutional Review Board at the respective host institutions. All study participants signed informed consent documents, and the study was performed in accordance with Health Insurance Portability and Accountability Act (HIPAA) Privacy Rules. DNA was extracted from peripheral blood leukocytes with salt extraction and genotyped with the Illumina Linkage IVb mapping panel.[1] LOD scores were calculated using easyLinkage-Plus software using genotype results of all consenting family members in the parental and affected generations.[2] Fine mapping of selected individuals was performed using the Affymetrix 250K Nsp1 SNP array and results analyzed using identity-by-descent mapping. Exome capture was performed using the Agilent SureSelect Human All Exome 50Mb Kit and paired-end sequenced on an Illumina instrument.[3] Depth of coverage was 30±16 (s.d) per exome and exome data was analyzed as previously described.[4] Whole exome sequencing for case II-1 family 3 was performed on an Illumina Hiseq 4000, using the SureSelect Human All Exon V6 enrichment kit and a paired-end 75bp sequencing protocol and data analysis and filtering for autosomal recessive inheritance was performed as previously described.[5]

Whole genome sequencing (WGS)

Both affected siblings from family 4 underwent whole genome sequencing. In brief, Sample prep (TruSeq DNA, input 250 ng) and the Illumina's HiSeqX sequencing platform were used according to manufacturer's instructions to perform WGS with 2x150bp read length. Illumina data were processed with the inhouse developed pipeline (https://github.com/hartwigmedical/pipeline), with settings validated for clinical genetics version 1.12 (https://github.com/hartwigmedical/pipeline/blob/master/settings/KG.ini).

The 20x coverage of the exome target sequence was >95% for all samples. Variants present in the protein coding region or those that potentially affect splicing, +/- 6 base pairs into the intron were prioritized using Cartagenia Bench Lab NGS (Agilent Technologies, Santa Clara, USA) based on population allele frequency and anticipated inheritance patterns. Further interpretation was performed based on predicted functional impact of the variants and literature.

For case II-3 from family 6, the DNA libraries for Trio-Whole Genome Sequencing were prepared for WGS using Illumina´s TruSeq PCR-Free sample preparation kit according to manufacturer instructions. In short, 1 μ g of gDNA was fragmented to a mean target size of 350-450 bp using a Covaris E220 instrument, followed by end-repair, 3'-adenylation and ligation of indexed sequencing adaptors. The quality and concentration of all sequencing libraries was assessed using a LabChip GX instrument (Perkin Elmer), followed by further quality control using a MiSeq sequencer (Illumina) to obtain optimal cluster densities, insert size and library diversities. Sequencing libraries (one sample per lane) were hybridized to the surface of HiSeqX flowcells (v2 or v2.5) using the Illumina cBot™. Paired-end sequencing-by-synthesis (SBS) was performed on Illumina HiSeqX sequencers, using 2x150 cycles of incorporation and imaging. Real-time analysis involved conversion of image data to base-calling in real-time. All steps in the sample preparation and sequencing workflow were monitored using an in-house laboratory information management system (LIMS) with barcode tracking of all samples and reagents.

The GRCh37 reference sequence was used to map reads. The raw sequences were aligned to reference sequence using BWA version 0.7.10. The sequences in the BAM files were realigned around indels with GATKLite version 2.3.9 using a public set of known indels. PCR duplicates marked with Picard tool version 1.117. We filtered out the

variants with low map quality, low read depth (<6x), low Phred-scaled SNP quality score (<20) and strong strand bias. Variants were analyzed using the Clinical Sequence Miner application (DeCODE Genetics, Iceland). Low-quality variants, variants with call ratios of less than 20%, and variants with global allele frequencies higher than 0.01 were excluded from analysis according to Exome Aggregation Consortium (ExAC), Genome Aggregation Database (GnomAD) and Greater Middle East Variome project (GME Variome). Variants were analyzed under the assumption of being present or homozygous in the affected individual and absent or heterozygous in the unaffected parents. Variants were prioritized according to *in silico* pathogenicity score using Phred-scaled score provided by Combined Annotation Dependent Depletion (CADD).

Reverse Transcription (RT) PCR

Fibroblasts from affected individuals were harvested from punch biopsy and grown as previously described.[6] For the relative quantification of mRNA expression, total RNA from quantified subject and control fibroblasts was reverse-transcribed using the Superscript III First-Strand cDNA Kit (Invitrogen). PCR analysis of cDNA was performed using dHPLC-purified primers designed against exons 4-6 of *ADPRHL2* excluding introns and PCR products were visualized using standard techniques.

Antibodies

ADPRHL2 (Sigma HPA027104); Tubulin (Sigma T6074).

Western Blot

Patient and healthy control fibroblasts were grown to 90% confluence, pelleted, and lysed in the treatment buffer (20mM Tris-HCl pH 8, 137mM NaCl, 1% Triton X-100, 2mM EDTA) with a cocktail of protease inhibitors (Complete Protease Inhibitor Cocktail

Tablets, Roche). Protein quantification was performed with the BCA Protein Assay Kit (Pierce), 25 µg of the protein samples were run on standard 10% SDS-PAGE gels, and transferred to a PVDF membrane. Membranes were then blocked in either 5% non-fat milk powder or 4% BSA in Tris-buffered saline Tween (TBST), incubated overnight in the primary antibody solutions, washed, and incubated in the HRP-conjugated secondary antibody solutions for 1 hour. Bands were visualized using an appropriate chemiluminescence detection reagent.

Protein Purification

Wildtype *ADPRHL2* cDNA was cloned into pET15b vector and mutations were introduced via mutagenesis with NEB Q5 mutagenesis kit. Recombinant proteins were purified with *Escherichia coli BL21-CodonPlus (DE3)-RIPL* competent cells (Agilent) according to previous study.[7]

Thermofluor Assay

6 µg of purified protein was re-buffered in Hepes buffer (10 mM Hepes; 1 mM $MgCl_2$; 5 % Glycerol; pH 7.0) and mixed with 10 x SYPRO™ Orange Protein Gel Stain in DMSO (Invitrogen™) to a total volume of 25 µl. 100 µM ligands (adenosine diphosphate ribose (ADPr); adenosine triphosphate (ATP); ribose-1-phosphat (r-1-P); ribose-5-phosphat (r-5-P)) were added to test their influence on the thermal stability. Triplicates were pipette in a 96 well plate, heated up to different temperatures in a rage of 15-70 °C and measured the fluorescence with Applied Biosystems 7500 Real-Time PCR System, using the ROX filter. Data were analyzed with Protein Thermal Shift™ Software (Thermo Scientific™).

Circular Dichroism (CD) Spectroscopy

40-50 µg purified protein were re-buffered in NaPO4 (10 mM; pH 7.0) and diluted in a total volume of 200 µl. Proteins were heated from 10°C to 70°C in 5-10°C steps in the range of 180-260 nm or with variable temperature from 10-70 °C (1°C/minute) while measuring the θ mdeg with the Jasco J-715 CD-spectrometer at 221 nm. Data were collected in cuvette with 1 mm path length and analyzed with DichroWeb using the CONTINLL algorithm and the reference set 7 (25; 26). Data were normalized for molarity to obtain the mean residual elipticity.

***Drosophila* Stocks and Crosses**

UAS-*Dicer* 2 (#24650), daughterless (*da*)-Gal4 (#5460), and *elav*-Gal4 (#458) were obtained from the Bloomington Stock Center (Indiana). Parg$^{27.1}$ was kindly provided by A. Tulin as described.[8] UAS-*parg* RNAi (#23964GD) was obtained from VDRC (Vienna). All Gal4 and UAS strains were out-crossed into w1118 at least 6 times. Flies were maintained at room temperature. Experiments were performed at 25°C. Dicer-2 (Dcr) was included in RNAi experiments together with *da*>Gal4 or elav-Gal4 to enhance RNAi effects.[9] Homozygous *elav*-Gal4; UAS-*Dcr* and *da*-Gal4;UAS-*Dcr* stocks were established by standard genetic crosses, then crossed to either to UAS-*parg* RNAi for RNA knock-down or to w1118 for control in respective experiments.[9]

Quantitative PCR (qPCR)

Total RNA was isolated from whole flies, heads, or bodies using Trizol (Invitrogen) and the RNeasy Mini Kit (Qiagen) according to the manufacturer's instructions. cDNA synthesis was performed with oligo-dT and random primers using SuperScript III first-strand synthesis system (Invitrogen). qPCR was performed in duplicate using SYBR

Green on an ABI 7900HT qPCR system (Applied Biosystems) according to the manufacturer's protocol. All samples were analyzed from at least 3 independent experiments. Data was normalized to the level of rp49 mRNA prior to quantifying the relative levels of mRNA between controls and experimentally treated samples.

Oxidative Treatment

Four to five day-old males, grouped with 20 flies per vial, were fed on a 3mm Whatman paper soaked with 1% hydrogen peroxide (Sigma) in 5% sucrose/PBS. Control flies were fed 5% sucrose/PBS. Under this condition, flies live up for 10 days without consequence. Scores were generated every 12 hours for the number of dead flies. Fresh hydrogen peroxide was added daily. For Minocycline experiments, flies were fed first with 5% sucrose/PBS or 5% sucrose/PBS/Minocycline for 24 hours prior to adding hydrogen peroxide (n=160 flies per genotype for all experiments).

Hypoxic Treatment

Male flies were collected within 24 hours of eclosion, placed at a density of 20 flies per vial, and aged for 2-3 days before subject to hypoxia. Flies were fed with standard food, maintained in a hypoxic chamber (COY Laboratory Products INC) filled with 2% oxygen at 22°C, and transferred every 2 day to new vials within the chamber without exposure to air, therefore avoiding re-oxygenation. The number of dead flies was scored daily (n=200 flies per genotype).

Lifespan

$Parg^{27.1}$ and w1118 flies were allowed to produce eggs and develop until second instar larvae at 25°C. The larvae were then transferred to an incubator at 29°C until eclosion. Adult flies were collected within 24 hours of eclosion, grouped 10 males per vial on

standard fly food, and placed back at 25°C. Flies were passed every day and dead flies were scored until all $Parg^{27.1}$ flies were dead (n=60 $Parg^{27.1}$ and n=120 w1118 flies).

Statistical Analyses

Survival was analyzed by Kaplan–Meier Log-rank Test, and gene expression was analyzed by the Student's t-test or One-way ANOVA with Dunnett's posttest using Graph Pad Prism4 software. $p < 0.05$ was considered statistically significant.

Supplemental References

1. Murray, S.S, Oliphant, A., Shen, R., McBride, C., Steeke, R.J., Shannon, S.G., Rubano, T., Kermani, B.G., Fan, J.B., Chee, M.S., et al. (2004). A highly informative SNP linkage panel for human genetic studies. Nat Methods 1, 113-117.
2. Hoffmann, K. & Lindner, T.H. (2005). easyLINKAGE-Plus--automated linkage analyses using large-scale SNP data. Bioinformatics 21, 3565-3567.
3. Gnirke, A., Melnikov, A., Maguire, J., Rogov, P., LeProust, E.M., Brockman, W., Fennell, T., Giannoukos, G., Fisher, S., Russ, C., et al. (2009) Solution hybrid selection with ultra-long oligonucleotides for massively parallel targeted sequencing. Nat Biotechnol 27, 182-189.
4. Dixon-Salazar, T.J., Silhavym J.L., Udpa, N., Schroth, J., Bielas, S., Schaffer, A.E., Olvera, J., Bafna, V., Zaki, M.S., Abdel-Salam, G.M., Mansour, L.A., et al (2012). Exome sequencing can improve diagnosis and alter patient management. Sci Transl Med 4, 138ra178.
5. Alawbathani S., Kawalia, A., Karakaya, M., Altmuller, J., Nurnberg, P., Cirak, S. (2018). Late diagnosis of a truncating WISP3 mutation entails a severe phenotype of progressive pseudorheumatoid dysplasia. Cold Spring Harb Mol Case Stud 4, a002139.
6. Villegas, J. & McPhaul, M. (2005). Establishment and culture of human skin fibroblasts. Curr Protoc Mol Biol Chapter 28, Unit 28 23.
7. Mueller-Dieckmann, C, Kernstock, S., Lisurek, M., von Kries, J.P., Haag, F., Weiss, M.S., Koch-Nolte, F. (2006). The structure of human ADP-ribosylhydrolase 3 (ARH3) provides insights into the reversibility of protein ADP-ribosylation. Proc Natl Acad Sci USA 103, 15026-31.
8. Hanai, S., Kanai, M., Ohashi, S., Okamoto, K., Yamada, M., Takahashi, H., Miwa, M. (2004). Loss of poly(ADP-ribose) glycohydrolase causes progressive neurodegeneration in Drosophila melanogaster. Proc Natl Acad Sci U S A 101, 82-86.
9. Dietzl, G., Chen, D., Schnorrer, F., Su, K.C., Barinova, Y., Fellner, M., Gasser, B., Kinsey, K., Oppel, S., Scheiblauer, S., et al (2007). A genome-wide transgenic RNAi library for conditional gene inactivation in Drosophila. Nature 448, 151-156.
10. Whitmore, L. and Wallace, B.A. (2004) DICHROWEB, an online server for protein secondary structure analyses from circular dichroism spectroscopic data. Nucleic Acids Res 32, W668-73.
11. Sreerama, N. and Woody, R.W. (2000). Estimation of protein secondary structure from circular dichroism spectra: comparison of CONTIN, SELCON, and CDSSTR methods with an expanded reference set. Anal Biochem 287, 252-60.